Shedding New Light on Black Holes with the Sloan Digital Sky Survey

John Parejko

Drexel University, Department of Physics

parejkoj@drexel.edu

Abstract

I present here the results of a multi-wavelength study of a sample of nearby galaxies in which emission line activity is exhibited to different degrees. There have been many studies of the luminosities and efficiencies of high luminosity accreting sources, such as quasars, but very few studies of lower luminosity sources such as Seyferts and LINERs. By using data from the Sloan Digital Sky Survey (SDSS), the Galaxy Evolution Explorer (GALEX), the Faint Images of the Radio Sky at Twenty-cm (FIRST), and the Röntgen Satellite (ROSAT), I have computed spectral energy distributions, and hence bolometric luminosities for a small sample of cross-matched objects. For this data set, using the stellar velocity dispersion–black hole mass relation, I have obtained estimates of the black hole masses in these systems, and derived Eddington ratios. I compare these results for different classes of objects, defined based on their spectral properties and also with calculations from previous studies. This study represents the basis for future, more detailed work that aims at filling in the gaps in the spectral energy distributions that are crucial for understanding physics behind the nuclear activity in these galaxies.

1. Active Galaxies and Super Massive Black Holes

There is increasingly strong evidence that nearly all galaxies contain supermassive black holes ($M_{BH} \geq 10^6 M_\odot$) in their centers, and that the evolution of the black hole and its host galaxy are tightly linked. A significant fraction of these black holes are actively accreting their surrounding material, the distant quasars being a common example. In the local universe we see activity similar to quasars, but at a much lower level. These low luminosity active galactic nuclei (AGN) may be the faded engines of formerly powerful quasars. Measuring the masses and accretion rates of the black holes that drive the low luminosity AGN will help us understand the evolution of these sources.

Since the initial description of active galaxies (Seyfert 1943), it has been found that roughly 20% of all galaxies have signatures of nuclear activity. AGN are now generally separated into the two main subclasses based purely on luminosity: quasars and Seyferts. Seyfert galaxies are observed to have strong emission lines and the brightest Seyferts are otherwise indistinguishable

from quasars. Seyfert type 1 galaxies are identified by the presence of broad lines super-imposed on the strong narrow emission lines, while type 2 Seyferts have no broad lines (Peterson 2003,p. 22). Historically, several sub-subclasses were defined – 1.2, 1.5, 1.8 – based on the relative strength or presence of different broad-lines, but these divisions have fallen out of favor.

The broad lines in type 1 Seyferts typically have full-width half-max (FWHM) of >1000km/s. This emission is thought to originate from a broad line region (BLR). The BLR is generally viewed as a group of hot gas clouds orbiting very near to the central black hole. Narrow lines characteristic of Seyfert 2s are thought to originate from the narrow line region (NLR), which produces lines with FWHM of only a few 100s km/s. The NLR is viewed as a low density torus orbiting much further out from the black hole. The low density of the NLR means that forbidden transitions are not collisionally supressed. The ratios of the corresponding forbidden lines are used to classify AGN.

Assuming the black hole driving the AGN has a mass M_{BH}, we can compare its expected luminosity with the observed luminosity of the central region of the galaxy. If the black hole is isotropically accreting at the maximum stable rate, known as the Eddington limit, its luminosity will be

$$L_{edd} = \frac{4\pi G c m_p}{\sigma_e} M_{BH}, \tag{1}$$

where $\sigma_e$is the Thomson scattering cross-section for electrons. (Peterson 2003,p. 33) Thus, if we can establish M_{BH} through some other means, we can calculate the Eddington ratio, L_{BH}/L_{edd}, which is a proxy for the accretion efficiency. Ho (1999) found Eddington ratios between 2×10^{-6} to 2×10^{-3} for his sample of 7 low-luminosity AGN which is low when compared to more distant and luminous systems. As AGN appear dimmer over time while their black holes are increasing in mass, their accretion rates must be falling. How this evolution varies with AGN class has yet to be explored; this work will investigate these issues in detail.

Unfortunately, it is very difficult to directly measure the mass of the central source in distant galaxies, owing to the extremely small size of the accreting region. We therefore require indirect methods to derive the mass of the central black holes in active galaxies. Some commonly used examples include assuming the motion of the broad-line clouds is virialized (reverberation mapping), and exploiting the black hole mass - bulge velocity dispersion relation, (Tremaine et al. 2002). These techniques generally require dedicated observing time on large telescopes, but with the advent of modern, large-scale surveys, we can combine multiwavelength observations (L_{bol}) and detailed spectra (σ_{bulge}), to find the Eddington ratios of a large set of low luminosity AGN.

I present here the results of a multi-wavelength study of a sample of nearby, low-luminosity, accreting supermassive black holes. The data for the current study comes from the Sloan Digital Sky Survey (SDSS), the Galaxy Evolution Explorer (GALEX), the Faint Images of the Radio Sky at Twenty-cm (FIRST) and the Röntgen Satellite (ROSAT). Currently lacking is data from the Infrared band, but I plan to include data from the Spitzer Space Telescope and the 2-Micron All Sky Survey (2MASS) in the future. Previous work on this subject involved a sample of only 7 nearby galaxies

(Ho 1999). With the upcoming release of the updated GALEX catalog, my sample should contain hundreds of emission-line galaxies, dozens of which will be identifiable as some class of AGN; many others could be have stronger classification based on the results of this study.

2. Plan for the Current work

- Start with a set of SDSS galaxies that were spectrally classified by (Constantin & Vogeley 2006).
- Match other surveys (GALEX, FIRST, ROSAT currently) with SDSS spectral objects and cross match between all surveys.
- Look for unique properties of each identified AGN class, if any.
- Compute an SED for each galaxy, given the spectral data from all the surveys, using proper upper-limits given the coverage maps.
- Compute the bolometric luminosity for each object, given the SED and redshift (z).
- Compute a black hole mass from the stellar velocity dispersion, and thus derive a maximum eddington luminosity.
- Compare L_{bol} and L_{edd} to compute the Eddington ratio.

3. Finding Low Luminosity AGN

Identification of AGN is a non-trivial task. The importance of viewing geometry, obscuration and absorption on the resulting spectrum means that one technique is not sufficient to locate **all** AGN. A large proportion of the observed x-ray background has been resolved by Chandra as optically obscured active nuclei (Treister et al. 2005). It is suspected that the ratio of optically obscured to observed AGN is 3:1. For this survey I used a classification system based on identifications of emission-lines in SDSS galaxies, as discribed in (Constantin & Vogeley 2006).

For this work, the galaxies were classified based on the presence or absence of emission-lines, and sub-classified based on comparisons of the following line ratios: [OIII]$\lambda 5007/\mathrm{H}\beta$, [NII]$\lambda 6583/\mathrm{H}\alpha$, [SII]$\lambda\lambda 6716, 6731/\mathrm{H}\alpha$, and [OI]$\lambda 6300/\mathrm{H}\alpha$(Constantin & Vogeley 2006). These ratios take advantage of the physical distinctions between the different classes.

4. Datasets

The survey overlap regions are shown in (fig. 1). GALEX cross-matches are localized to the regions that were imaged for GR1, and most of those regions were part of the AIS. FIRST detections are uniformly spread across nearly the entire SDSS field, with only a small piece missing from the northern-most area. The small number of ROSAT cross-matches are difficult to see and more concentrated toward the north, where the exposure time was greater.

4.1. SDSS

The baseline dataset for this study is the Sloan Digital Sky Survey (SDSS) spectroscopic data from the SDSS Data Release 4 (DR4) (Adelman-McCarthy & et al 2005). A magnitude-limited subsample of the DR4 galaxy catalog was selected with 14.5 < m_r< 17.7 which removes those bright galaxies which are normally broken into multiple components by the SDSS pipeline. Next, a volume-limited subsample was produced, with a redshift limit of 0.05 < z < 0.12. Volume-limiting the sample is not necessary for this study, but it is the only data available at this time. The galaxies were then classified as described above. This initial setup was done by Constantin & Vogeley (2006).

4.2. GALEX

The Galaxy Evolution Explorer (GALEX) spacecraft, launched in April 2003, was designed with a goal of providing high-resolution (~arcsecond), wide-field (~1 square-degree) near and far ultra-violet imaging. The first large public data release, Galex Release 1 (GR1) occured in December 2005. GR1 covered ~2939 square degrees of sky, split between the All (AIS), Medium (MIS) and Deep (DIS) Imaging Surveys. The majority of this coverage was in the AIS, which has an average depth of 121 seconds.

The GALEX spacecraft imaging system has a roughly 1.2 degree diameter, circular field of view. This consists of two fields (listed to 10% fall-off): near UV spanning 134 - 179 nm and far UV spanning 171 - 283 nm. The photometric radial error, found by comparing with known star positions from Hipparcos, is ~1.1" for the Far UV and ~1.2" for the Near UV for GR1.

Unlike the other surveys in this study, the GALEX surveys were not designed with completely uniform coverage in mind, so many fields were imaged multiple times and not all fields have uniform exposure, even within the AIS. The GALEX database does not yet have a system for identifying objects that were imaged in more than one field. Thus, there are >14000 cases where an SDSS object has more than one GALEX object matched to it, out of ~34600 total matches 1. For the future, I will select the "best" GALEX object based on the exposure time of the given frame, but the current analysis takes only those SDSS objects with unique matches in GALEX. A

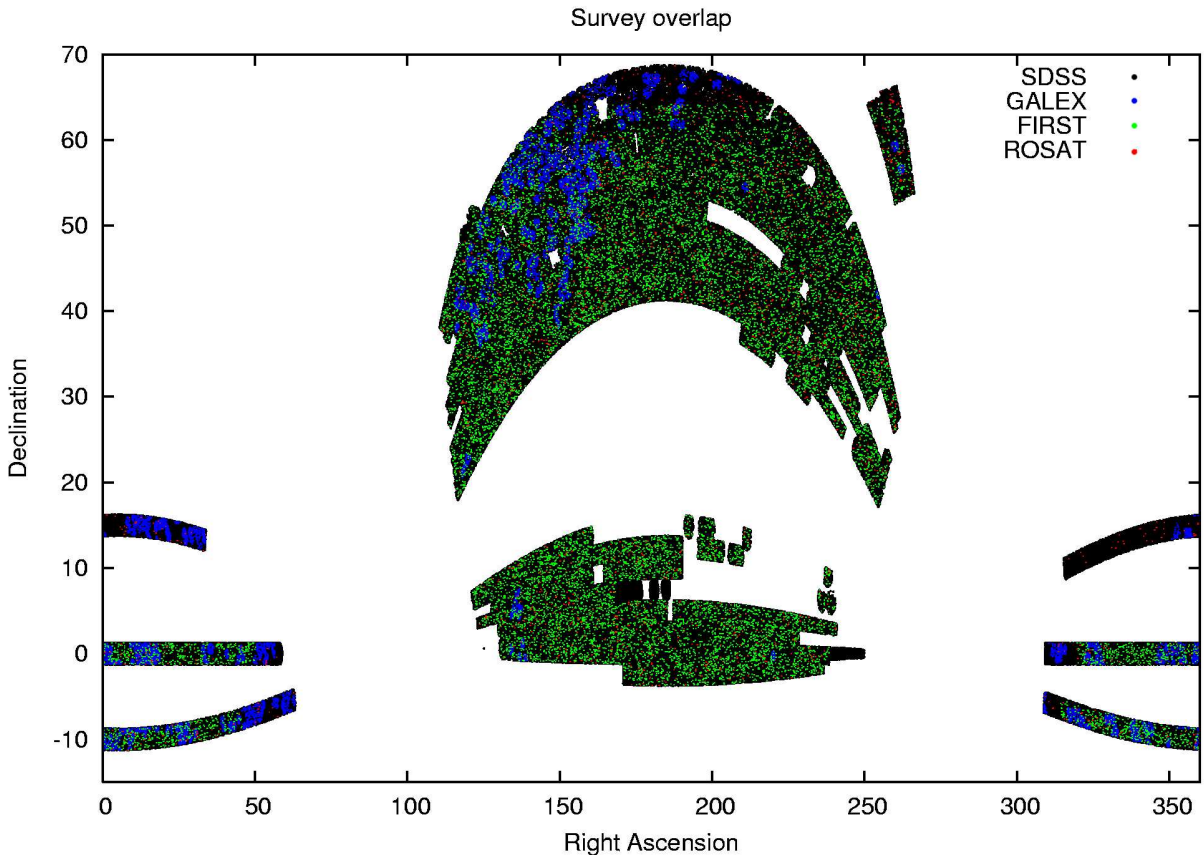

Fig. 1.— Each unique detection from the three surveys is overplotted on the entire set of SDSS galaxies that were considered in this survey. Note that only cross-matching detections are shown, not the complete survey overlaping regions, where upper-limits are available.

possible follow-up study would use these multiple-imagings to reduce the GALEX astrometric error, though this may already be in the works for the GR2.

For comparison, the mean and standard-errors are shown (table 2) for the separation, fluxes and magnitudes of passive (absorption) galaxies, all emission galaxies, HII galaxies, Seyferts and LINERs. Notice that the brightest galaxies are the HII, followed by Seyferts, LINERs and finally those galaxies with no emission, as would be expected. Also notice that there is little difference between the SDSS/GALEX separations between the various classes, implying that the number of chance superpositions or non-central GALEX objects is rather small.

4.3. FIRST

The Faint Images of the Radio Sky at Twenty-cm (FIRST) survey, begun in 1994, provides a complete radio map of the northern sky at 21cm. It is essentially complete as of April 2003. There is now a catalog available, containing all extracted sources down to a limiting magnitude of roughly 1 mJy, with 5 arcsec resolution. (Becker et al. 1995) This catalog contains over 800,000 objects, covering 9033 square degrees of sky. A complete coverage map is available, which I will use for a more detailed analysis of the source upper-limits.

Nearly all of the SDSS sky coverage overlaps with FIRST, and the FIRST astrometric precision of <1" is well matched for cross-correlating radio and SDSS optical sources. Because of this, and the fact that the FIRST survey was complete by the SDSS Data Release 2 (DR2), part of the SDSS analysis pipeline includes cross-matching with FIRST objects. SDSS photometric objects which have a FIRST match are also flagged for possible inclusion in the spectroscopic follow-up studies.

As shown in (table 3), the LINERs are by far the brightest sources, followed by Seyferts, though there is a large scatter in the fluxes of each. Note also that only 6 of the passive galaxies in this sample have a detected radio flux, and those that are detected are the dimmest on average. It is also interesting to note that the Seyferts have nearly half the separation between the SDSS and FIRST detections, compared with the other galaxy types.

4.4. ROSAT

The oldest of the utilized surveys, the Röntgen Satellite entered orbit in June 1990. The release of the ROSAT All Sky Survey (RASS) in 1999 (Voges et al. 1999), provides the deepest, greatest sky-coverage x-ray survey currently available. The survey catalog provides a count rate (per second) and two hardness ratios for each detected target. the hardness ratios are between the soft (0.1-0.4 keV) and hard (0.5-2.0 keV) bands for hard1 and between 0.5-0.9 keV and 0.9-2.0 keV for hard2. Unfortunately, the survey imager - the Position Sensitive Proportional Counter (PSPC) - had a PSF of ~20 arcsec. This, combined with the pointing precision, meant that the location of x-ray sources

Table 1: Summary of the surveys.

	GALEX	FIRST	ROSAT
SDSS DR4 overlap (sq. deg.)	TBD	6600	6600
wavelength range	134-179nm, 171-283nm	21cm	0.1-2.4keV
upper-limit (nominal, 5σ)	(*)	1 mJy	0.01cps (*)
PSF resolution	4″	5″	~20″
astrometric precision	1.1″	<1″	~30″
SDSS DR4 matches (total)	34616	18238	2837
SDSS DR4 matches (unique)	20508	18226	2059

Note. — (*) There is no defined GALEX upper-limit, because the exposure time varies significantly between fields. The ROSAT upper-limit is very rough, for the same reason. A more detailed analysis of the upper-limits for these surveys will be performed at a later date.

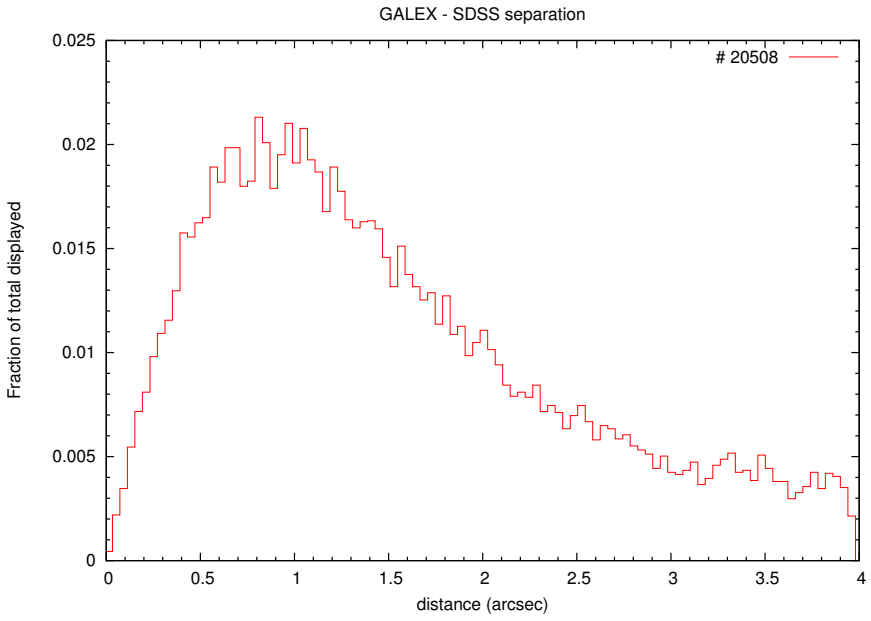

Fig. 2.— The separations between all unique GALEX/SDSS galaxy matches. This is consistent with the measured GALEX astrometric error of ~1.1″: most of the GALEX matches are within 1.5″ of the corresponding SDSS object. However, it is quite possible that separations greater than 1″ represent distinct objects. For an example, see (fig. 5).

Table 2: Selected GALEX statistics: mean+σ (median).

class (total)	separation (")	NUV flux (μJy)	FUV flux (μJy)	NUV mag	FUV mag
passive (297)	1.66±0.5 (1.5)	18.0±2.0 (6.8)	21.2±2.7 (10.6)	21.6±0.1 (21.8)	21.4±.1 (21.3)
emission (1308)	1.30±0.03 (1.08)	52.4±1.5 (37.5)	36.5±1.1 (25.45)	20.0±0.03 (20.0)	20.4±0.03 (20.4)
HII (822)	1.16±0.03 (1.01)	61.9±1.9 (49.2)	40.7±1.4 (30.6)	19.7±0.03 (19.7)	20.2±0.03 (20.2)
Seyfert (58)	1.36±0.11 (1.17)	34.9±7.8 (14.4)	27.4±7.9 (10.9)	20.7±0.2 (21.0)	21.0±0.2 (21.3)
LINER (223)	1.70±0.07 (1.38)	29.8±2.9 (16.6)	23.5±2.9 (11.9)	20.8±0.08 (20.1)	21.1±0.1 (21.2)

Note. — The total is the number of objects within all the survey regions. Separation is the distance between the SDSS spectral object and the GALEX detection central position. Passive galaxies are those with absorption lines and no detectable emission.

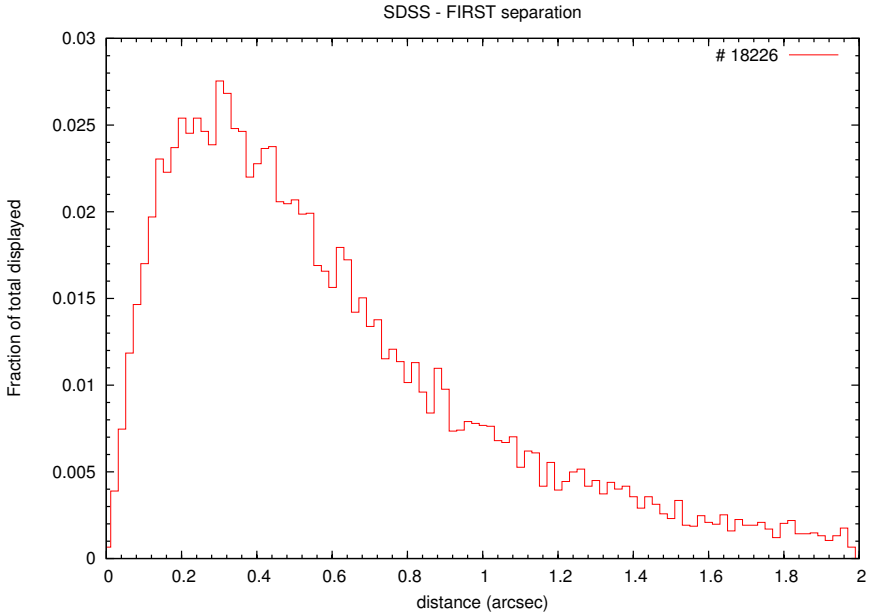

Fig. 3.— The separations between all unique FIRST/SDSS galaxy matches. The FIRST astrometric solutions are good to a fraction of an arcsecond, which is plainly apparent in the separation between the FIRST and SDSS objects. Considering that most bright radio emission is expected to come from the galaxy's core, this tight relation bodes well for reducing spurious matches.

was only known to within half an arcminute. Though very good for an x-ray survey, it is the weak link in this work.

Within the ~60" ROSAT error circle, there are potentially several SDSS detected galaxies. There is no way to determine which of these objects is the true x-ray source, even in the cases where more than one cross-matched SDSS galaxy has a spectrum. In roughly 400 cases, more than one SDSS spectrally observed galaxy was matched to a single ROSAT detection. This is potentially quite significant, since the number of unique ROSAT-SDSS galaxy matches is just over 2000.

Table 4 shows statistics for all ROSAT/SDSS matches. It was necessary to use all matched objects from the ROSAT catalog, not just those restricted to the GALEX targeted regions, because of the small number of total ROSAT/SDSS matched objects. If this list were restricted to only the regions where all the surveys overlapped, there would be only 13 emission-line galaxies, 2 passive, 5 H II, 1 Seyfert and 2 LINERs. This sample size is much too small to generate useful statistics. From the table, it appears the LINERS have a slightly harder flux than the other galaxies, and the HIIs have a slightly softer flux, but there seems to be little other difference.

4.5. Examples

Fig. 5 shows some examples of the matched objects and survey overlaps. Notice the large size of the ROSAT error circle relative to the SDSS object. The GALEX objects cover the entire SDSS-detected galaxies, and thus represent the integrated light from the entire galaxy. For ellipticals, the contribution from stars will be relatively small, but for any galaxy with active star formation, a significant fraction of the UV light will be from starlight. Some method of subtracting this excess light will be necessary, if we are to find the flux from only the central source.

Table 3: Selected FIRST statistics: mean+σ (median).

class (total)	separation (")	Integrated flux (mJy)	Peak Flux (mJy)
passive (6)	0.630±0.07 (0.694)	2.11±0.38 (1.91)	1.54±0.17 (1.50)
emission (183)	0.583±0.03 (0.462)	3.36±.46 (2.13)	3.02±0.45 (1.58)
HII (94)	0.652±0.04 (0.518)	2.38±0.16 (2.08)	1.87±0.14 (1.37)
Seyfert (18)	0.387±0.08 (0.319)	4.81±1.6 (2.21)	4.72±1.5 (2.03)
LINER (34)	0.531±0.07 (0.357)	6.41±2.2 (2.50)	6.13±2.1 (2.26)

Note. — The total is the number of objects within all the survey regions. Separation is the distance between the SDSS spectral object and the FIRST gaussian centroid. Passive galaxies are those with absorption lines and no detectable emission.

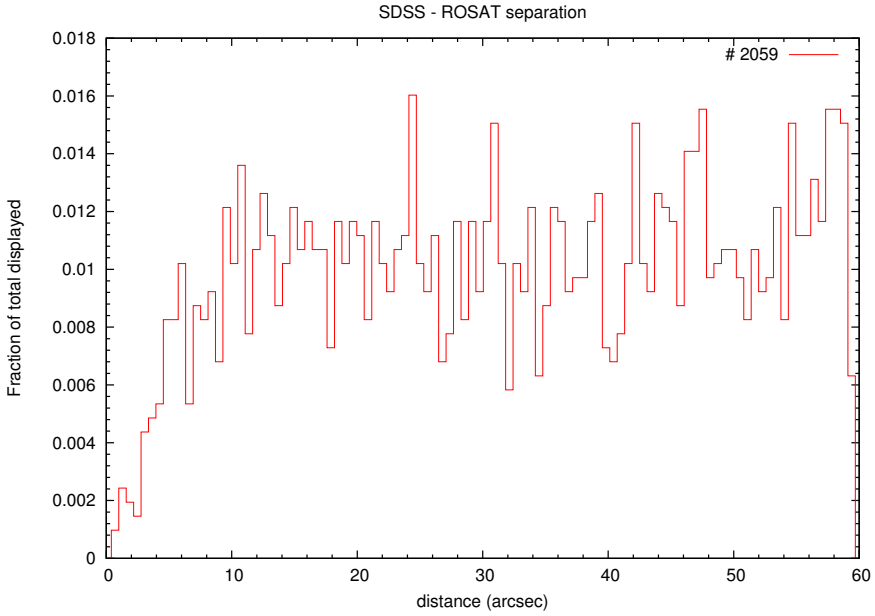

Fig. 4.— The separations between all unique ROSAT/SDSS galaxy matches. The 30″ ROSAT error circle means the separation between SDSS and ROSAT objects is by far the largest of the used surveys.

Table 4: Selected ROSAT statistics: mean+σ (median).

class (total)	separation (“)	counts/s	hardness 1	hardness 2
passive (51)	36.4±2.4 (34.1)	0.033±0.004 (0.024)	0.163±0.09 (0.22)	0.056±0.08 (0.05)
emission (126)	27.3±1.6 (24.4)	0.042±0.004 (0.029)	0.136±0.052 (0.135)	0.045±0.05 (0.09)
HII (49)	26.6±2.5 (21.8)	0.046±0.006 (0.029)	0.029±0.08 (0.0)	-0.02±0.08 (0.09)
Seyfert (15)	31.9±5.0 (28.9)	0.037±0.008 (0.025)	0.187±0.13 (0.16)	0.20±0.12 (0.16)
LINER (23)	32.1±3.5 (33.9)	0.041±0.01 (0.031)	0.303±0.14 (0.46)	0.09±0.12 (0.08)

Note. — The total is the number of SDSS objects uniquely matched to ROSAT objects. Separation is the distance between the SDSS spectral object and the ROSAT object center. Passive galaxies are those with absorption lines and no detectable emission.

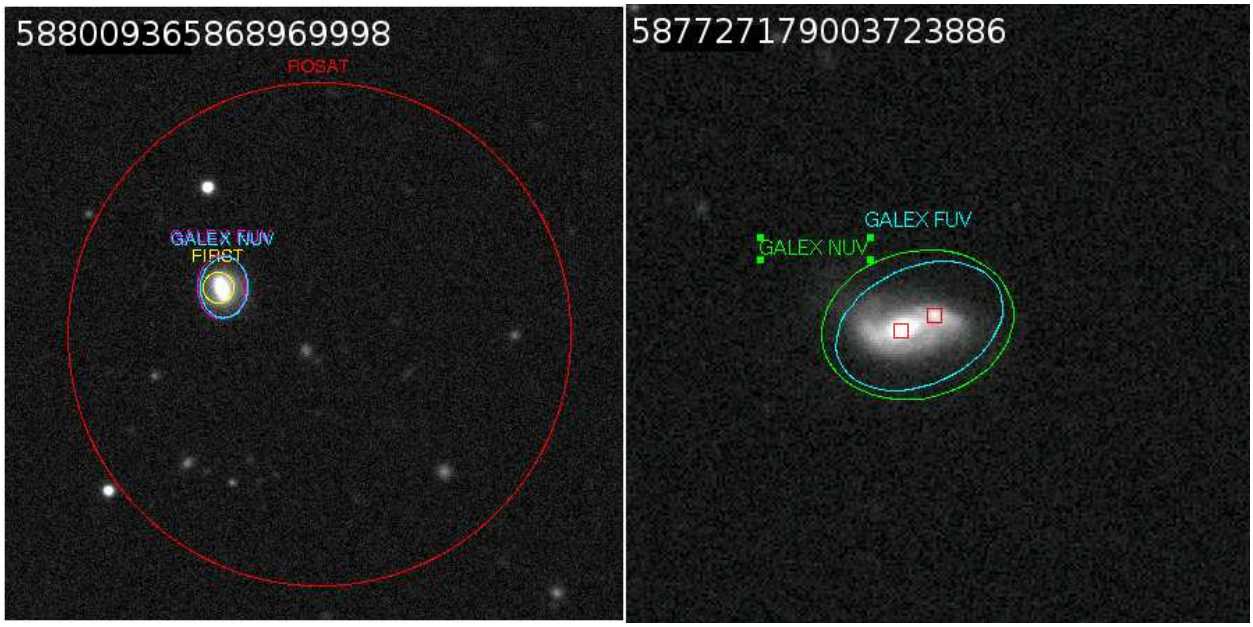

Fig. 5.— Error circles and detection examples. The numbers are the ObjIds in SDSS, for reference. The grey-scale image is the SDSS r-band. On the left is an unclassified emission-line galaxy with detections in each measured band. Several of the objects within the ROSAT error circle may be high-redshift galaxies. On the right is a spiral with with two SDSS spectra and the GALEX detections overplotted. The GALEX sources obviously encompass the entire galaxy, and are more likely associated with the star-forming regions than the core.

5. Spectral Energy Distributions

For comparison with previous work, I have plotted all the galaxies with ROSAT detections in (fig. 6). The high luminosity of the infrared region is plainly apparent in the data from Ho (1999). Also, the Ho galaxy SEDs are not as "smooth" as one would expect; this is due an ambiguity as to which fluxes he used when generating his results. Multiple fluxes are listed in his tables but not all of them were used. However, my bolometric luminosities for the Ho galaxies, computed from the plotted data, are all within a factor of 3 of his.

Few of my listed objects have FIRST detections (rough upper-limits are plotted), but because of the small size of this sample (and because I have only one Seyfert galaxies with a ROSAT detection, currently) no conclusions should be drawn from this. The data is limited by the small sky coverage of the GALEX GR1; the soon to be released GR2 will greatly increase the number of available sources.

Since all of my galaxies are significantly further away (148Mpc - 350Mpc) compared with those from Ho (1999) (3.6 - 92.0 Mpc), their comparable optical fluxes translate into signficantly higher luminosities (fig. 7). The high luminosity may be due, in part, to contamination from stars and star forming regions. Note that some of my objects do have UV detections (primarily unclassified emission-line and H II galaxies), while the UV luminosities from Ho are all much lower. Integrating the luminosity over the measured ranges gives the bolometric luminosities shown in tables 5-10. In these tables, objects are listed by SDSS objid, so the objects can be examined at the SDSS explorer website[1].

[1]SDSS Explore Home: http://cas.sdss.org/astro/en/tools/explore/obj.asp - use the "Search by ObjId" on the left panel to examine a given object.

Table 5: Unclassified galaxies

SDSS objid	D (Mpc)	L_{bol}(erg/s)	σ(km/s)	M_{BH} ($M_\odot$)	L_{edd}	L_{bol}/L_{edd}
587724233174876327	231	7.83×10^{42}	172	7.37×10^{7}	9.27×10^{45}	8.45×10^{-4}
587725773995835609	300	8.97×10^{42}	165	6.25×10^{7}	7.86×10^{45}	1.14×10^{-3}
587731186736300068	167	7.60×10^{42}	155	6.35×10^{7}	7.98×10^{45}	9.52×10^{-4}
587726878880629048	183	6.64×10^{42}	157	5.08×10^{7}	6.38×10^{45}	1.04×10^{-3}
588016893323247714	186	1.36×10^{43}	221	2.03×10^{8}	2.56×10^{46}	5.32×10^{-4}
588015509274427533	338	1.36×10^{43}	217	1.87×10^{8}	2.34×10^{46}	5.79×10^{-4}
587732580978065460	277	1.60×10^{43}	199	1.32×10^{8}	1.66×10^{46}	9.61×10^{-4}

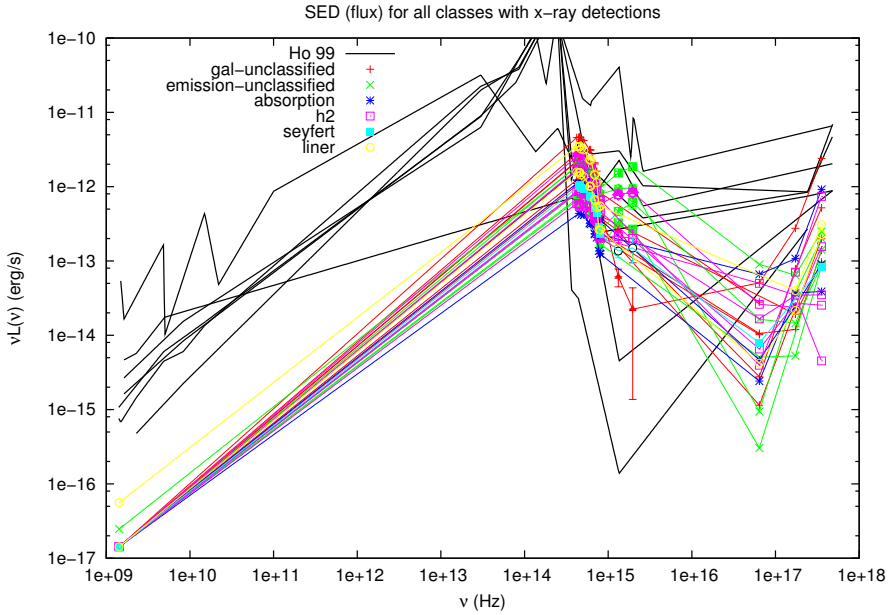

Fig. 6.— All the objects with ROSAT detections, color-coded by galaxy class. The black lines are the un-normalized SEDs from (Ho 1999). Note the large IR bump, which is missing from my data.

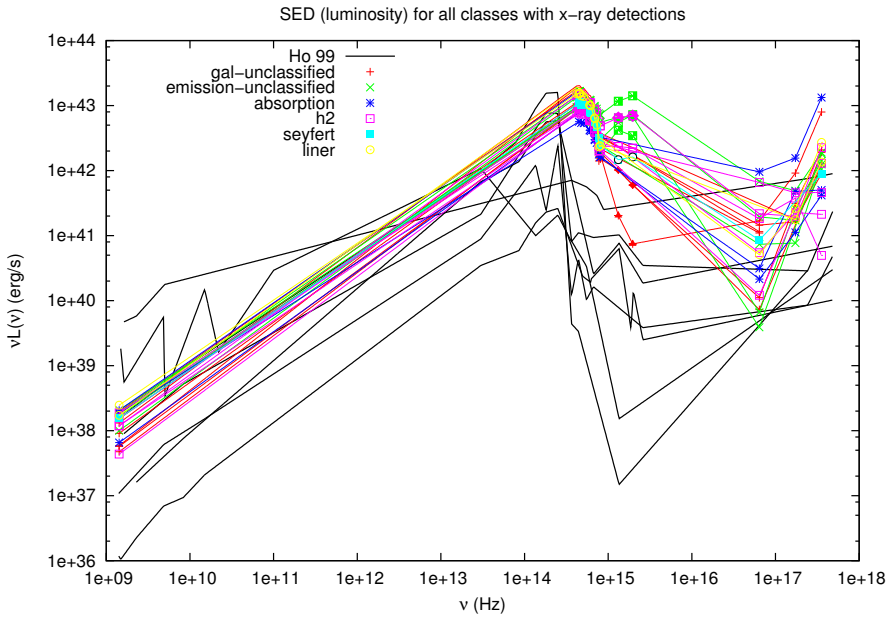

Fig. 7.— All the objects with ROSAT detections, color-coded by galaxy class. The black lines are the un-normalized SEDs from (Ho 1999). Note that my galaxies have a much higher optical flux, and several also have UV detections. This may be due to contamination from starlight, since the observation aperature is larger, and the galaxies are further away.

Table 6: Unclassified emission-line galaxies

SDSS objid	D (Mpc)	L_{bol}(erg/s)	σ(km/s)	M_{BH} ($M_\odot$)	L_{edd}	L_{bol}/L_{edd}
587724198274662549	348	8.11×10^{42}	109	1.16×10^{7}	1.46×10^{45}	5.56×10^{-3}
587724233182609470	242	1.33×10^{43}	134	2.73×10^{7}	3.43×10^{45}	3.90×10^{-3}
588015509269708902	314	1.20×10^{43}	146	3.79×10^{7}	4.77×10^{45}	2.51×10^{-3}
587725551211905117	328	8.37×10^{42}	180	8.86×10^{7}	1.11×10^{46}	7.52×10^{-4}
588009365868969998	252	2.17×10^{43}	600	1.12×10^{10}	1.40×10^{48}	1.55×10^{-5}

Table 7: Passive (absorption) galaxies

SDSS objid	D (Mpc)	L_{bol}(erg/s)	σ(km/s)	M_{BH} ($M_\odot$)	L_{edd}	L_{bol}/L_{edd}
587724199349715113	329	5.01×10^{42}	74.3	2.52×10^{6}	3.16×10^{44}	1.59×10^{-2}
587727178985701469	196	5.81×10^{42}	118	1.64×10^{7}	2.07×10^{45}	2.81×10^{-3}
587727214419771685	347	1.67×10^{43}	214	1.75×10^{8}	2.21×10^{46}	7.56×10^{-4}

Table 8: H II galaxies

SDSS objid	D (Mpc)	L_{bol}(erg/s)	σ(km/s)	M_{BH} ($M_\odot$)	L_{edd}	L_{bol}/L_{edd}
588007005234331723	160	6.16×10^{42}	139	3.15×10^{7}	3.96×10^{45}	1.56×10^{-3}
588010137339625611	264	1.54×10^{43}	145	3.75×10^{7}	4.72×10^{45}	3.26×10^{-3}
587724232636497959	264	7.16×10^{42}	118	1.63×10^{7}	2.06×10^{45}	3.48×10^{-3}
587731185650762193	303	8.68×10^{42}	116	1.48×10^{7}	1.87×10^{45}	4.65×10^{-3}
588016892249964727	332	8.78×10^{42}	119	1.65×10^{7}	2.08×10^{45}	4.22×10^{-3}

Table 9: Seyferts

SDSS objid	D (Mpc)	L_{bol}(erg/s)	σ(km/s)	M_{BH} ($M_\odot$)	L_{edd}	L_{bol}/L_{edd}
588015509270495360	301	9.06×10^{42}	129	2.35×10^{7}	2.95×10^{45}	3.07×10^{-3}

Table 10: LINERs

SDSS objid	D (Mpc)	L_{bol}(erg/s)	σ(km/s)	M_{BH} ($M_\odot$)	L_{edd}	L_{bol}/L_{edd}
587726877812916234	192	1.25×10^{43}	244	3.0×10^{8}	3.77×10^{46}	3.33×10^{-4}
588015509276065938	318	1.43×10^{43}	223	2.08×10^{8}	2.62×10^{46}	5.44×10^{-4}

6. Black Hole Masses

Tremaine et al. (2002) derive a relation between M_{BH} and the stellar velocity dispersion of the galaxy σ of

$$log(M_{BH}/M_{\odot}) = \alpha + \beta log(\sigma/\sigma_0),$$

where $\sigma_0$is a reference value, taken to be 200km/s. In their analysis of 21 nearby galaxies which have detailed measurements of the central region, they find best fit values of

$$\alpha = 8.13 \pm 0.06,\ \beta = 4.02 \pm 0.32,$$

which I use in this study. A future study could examine how much the variations in α and β change the computed black hole masses, as there are other good-fit values quoted in Tremaine et al. (2002).

As seen in tables 5-10, the computed Eddington ratios are within the ranges given in (Ho 1999), (2×10^{-6} - 2×10^{-3}). However, most of mine are consistently high, which I believe is due to contamination from starlight, and possibly background x-ray sources. In particular, note the nearly uniform ~$3 \times 10^{-3} L_{bol}/L_{edd}$ for the H II galaxies; this is almost certainly due to contamination from star-forming regions. For this sample, I do not have enough objects to compile statistics on the different classes, but I will examine how the Eddington ratios vary with galaxy class in the follow-up study.

7. Future directions

Just recently, an HST archival proposal was submitted (Ho 2005), to combine high resolution HST, VLA and Chandra data to find the SEDs of other nearby low-luminosity AGN. This is a complementary study, as it will measure only the nuclear region of these AGN, but will likely have fewer total objects. It will provide a useful comparison for my results.

In the near future, the first XMM-slew survey data will be released. This survey will provide positional accuracy of a few arcseconds (Read et al. 2005), a depth comparable to ROSAT in the soft (0.1-2keV) x-ray region, and orders of magnitude better depth in hard (>2keV) x-rays than any previous survey(Freyberg et al. 2005). I intend to make use of the XMM-slew data as soon as it becomes available.

A very important region of the spectrum that is, unfortunately, missing from my data is infrared. Since dust and dust clouds contribute to a significant fraction of the output of AGN, I will need to fill this in. The 2-Micron All Sky Survey, and the Spitzer Wide-area InfraRed Extragalactic (SWIRE) surveys both can potentially fill the gap, but I do not yet have cross-matches between these two surveys and the SDSS. 2MASS is a much lower resolution, shallower survey, so no attempt has yet been made to cross-correlate it, while Spitzer does not yet have good tools for preparing and examining large catalogs derived from its observations.

REFERENCES

Adelman-McCarthy, J. K. & et al. 2005, The Fourth Data Release of the Sloan Digital Sky Survey

Becker, R. H., White, R. L., & Helfand, D. J. 1995, ApJ, 450, 559

Constantin, A. & Vogeley, M. 2006, ApJ, in review

Freyberg, M. J., Altieri, B., Bermejo, D., Esquej, M. P., Lazaro, V., Read, A. M., & Saxton, R. D. 2005, The XMM-Newton Slew Survey: a wide-angle survey in the 0.2 - 12 keV band

Ho, L. 2005, in HST Proposal, 6980–+

Ho, L. C. 1999, ApJ, 516, 672

Peterson, B. H. 2003, An Introduction to Active Galactic Nuclei (Cambridge University Press)

Read, A. M., Saxton, R. D., Esquej, M. P., Freyberg, M. J., & Altieri, B. 2005, The XMM-Newton Slew Survey

Seyfert, C. K. 1943, ApJ, 97, 28

Treister, E., Urry, C. M., & Lira, P. 2005, ArXiv Astrophysics e-prints

Tremaine, S., Gebhardt, K., Bender, R., Bower, G., Dressler, A., Faber, S. M., Filippenko, A. V., Green, R., Grillmair, C., Ho, L. C., Kormendy, J., Lauer, T. R., Magorrian, J., Pinkney, J., & Richstone, D. 2002, ApJ, 574, 740

Voges, W., Aschenbach, B., Boller, T., Bräuninger, H., Briel, U., Burkert, W., Dennerl, K., Englhauser, J., Gruber, R., Haberl, F., Hartner, G., Hasinger, G., Kürster, M., Pfeffermann, E., Pietsch, W., Predehl, P., Rosso, C., Schmitt, J. H. M. M., Trümper, J., & Zimmermann, H. U. 1999, A&A, 349, 389